THE JOURNAL OF PHYSICAL CHEMISTRY LETTERS
A JOURNAL OF THE AMERICAN CHEMICAL SOCIETY

pubs.acs.org/JPCL

Letter

Multiset Variational Quantum Dynamics Algorithm for Simulating Nonadiabatic Dynamics on Quantum Computers

Jingjing Li, Weitang Li, Xiaoxiao Xiao, Limin Liu, Zhendong Li, Jiajun Ren,* and Weihai Fang

Cite This: *J. Phys. Chem. Lett.* 2025, 16, 3911−3919

Read Online

ACCESS | Metrics & More | Article Recommendations | Supporting Information

ABSTRACT: Accelerating quantum dynamical simulations with quantum computing has received considerable attention but remains a significant challenge. In variational quantum algorithms for quantum dynamics, designing an expressive and shallow-depth parametrized quantum circuit (PQC) is a key difficulty. Here, we propose a multiset variational quantum dynamics algorithm (MS-VQD) tailored for nonadiabatic dynamics involving multiple electronic states. The MS-VQD employs multiple PQCs to represent the electronic−nuclear coupled wave function, with each circuit adapting to the motion of the nuclear wavepacket on a specific potential energy surface. By simulating excitation energy transfer dynamics in molecular aggregates described by the Frenkel−Holstein model, we demonstrate that the MS-VQD achieves the same accuracy as the traditional VQD while requiring significantly shallower PQCs. Notably, its advantage increases with the number of electronic states, making it suitable for simulating nonadiabatic quantum dynamics in complex molecular systems.

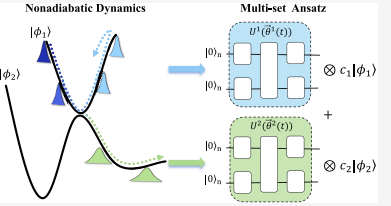

Nonadiabatic dynamics play a crucial role in chemistry, physics, and material science, influencing processes such as photochemical reactions, excitation energy transfer, charge separation, and relaxation.[1−4] In these processes, quantum effects, including coherence and tunneling, have been identified as essential.[5−7] However, accurately simulating nonadiabatic dynamics with quantum effects remains a major challenge in theoretical chemistry.[8,9] In classical computation, exact methods for solving the coupled electron−nuclear time-dependent Schrödinger equation (TDSE) suffer from exponential growth in complexity and memory with increasing system size, known as the "quantum exponential wall". Over the past few decades, various approximate but numerically exact methods have been developed to overcome this problem and have yielded great success.[10−14] However, their scalability and general applicability must be carefully assessed.

The advent of quantum computing offers compelling new avenues to overcome these challenges.[15−21] Simulating the TDSE is considered one of the most promising applications for demonstrating quantum advantage.[22] To this end, various quantum algorithms have been proposed,[23] including decomposition algorithms and variational algorithms.[22,24−33] Their applications to different chemical dynamics problems have also emerged, for both closed and open systems.[34−49] Compared with decomposition algorithms, hybrid quantum−classical variational algorithms require significantly shallower circuit depths and exhibit greater resilience to noise, making them more practical for implementation on near-term quantum hardware. Their feasibility has been validated in recent experimental demonstrations.[38,42,50]

In variational quantum algorithms,[51,52] the wave function ansatz, implemented as a parametrized quantum circuit (PQC), plays a crucial role in determining both accuracy and efficiency. An effective PQC must satisfy two key criteria: (i) high expressivity, enabling it to represent highly entangled quantum states beyond classical ansatzes, and (ii) short circuit depth, ensuring practical implementation on the current noisy quantum hardware. To meet these requirements, various PQC designs have been proposed,[53−63] including the unitary coupled cluster ansatz for electronic structure problems,[53] the Hamiltonian variational ansatz,[54] the hardware-efficient ansatz,[55] the quantum−classical hybrid ansatz,[59,63] etc.

Current variational quantum dynamics (VQD) algorithms use a single PQC, $U(\vec{\theta}(t))$, to represent the wave function of the entire system[18,27]

$$|\Psi(t)\rangle_{\mathrm{VQD}} = U(\vec{\theta}(t))|0\rangle \tag{1}$$

In nonadiabatic dynamics involving multiple electronic states, $U(\vec{\theta}(t))$ entangles both electronic and nuclear degrees of freedom. However, when potential energy surfaces (PESs) have distinct landscapes, the motion of the nuclear wavepacket on each PES varies significantly, making it difficult for a single compact PQC to accurately capture the full dynamics. A schematic example is shown in Figure 1a, where an initial nuclear wavepacket splits into two after passing through a strong nonadiabatic coupling region. On the steeper upper PES, the wavepacket reflects backward, while at the flatter lower PES, it propagates forward. In order to accurately

Received: March 11, 2025
Revised: April 2, 2025
Accepted: April 4, 2025
Published: April 10, 2025

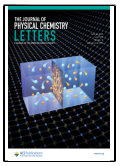

https://doi.org/10.1021/acs.jpclett.5c00739
J. Phys. Chem. Lett. 2025, 16, 3911−3919

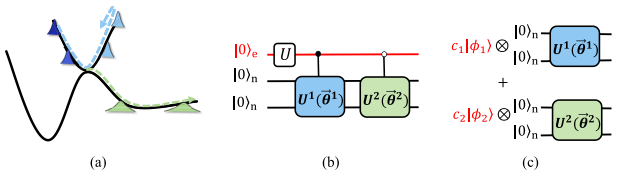

Figure 1. (a) Schematic illustration of a two-state nonadiabatic dynamics process. One wavepacket splits into two upon passing through a strong nonadiabatic coupling region. (b) In variational quantum dynamics, two distinct ansatz blocks are employed, determined by the electronic state index, resulting in a doubled circuit depth. (c) In multiset variational quantum dynamics, two separate circuits are used, each representing the nuclear wavepacket on a specific potential energy surface.

describe the two wavepackets, the PQC should incorporate two distinct ansatz blocks, $U^1(\vec{\theta}^1(t))$ and $U^2(\vec{\theta}^2(t))$, controlled by the qubit encoding the electronic state (Figure 1b), resulting in a doubled circuit depth.

To address this challenge, in this study, we proposed a multiset variational quantum dynamics algorithm (MS-VQD), an extension of the original VQD framework tailored for multistate dynamics, inspired by the classical multiset tensor network ansatz.[64] We demonstrated the effectiveness of the MS-VQD in simulating excitation energy transfer (EET) dynamics in molecular aggregates described by the Frenkel–Holstein model. EET plays a fundamental role in light-harvesting complexes and organic solar cells.[3,5] Our results showed that the MS-VQD achieves the same accuracy as the conventional VQD while requiring significantly shallower PQCs. Notably, its advantage becomes more pronounced as the number of electronic states increases, making it particularly well-suited for complex nonadiabatic quantum dynamics simulations.

The wave function ansatz of MS-VQD is

$$|\Psi(t)\rangle_{\text{MS-VQD}} = \sum_p c_p(t)|\phi_p\rangle_e|\chi_p(t)\rangle_n \tag{2}$$

$$|\chi_p(t)\rangle_n = U^p(\vec{\theta}^p(t))|0\rangle_n \tag{3}$$

where the subscripts e and n indicate electronic and nuclear wave functions, respectively. The MS-VQD employs separate PQCs, $U^p(\vec{\theta}^p(t))$, each independently representing nuclear wavepacket $|\chi_p\rangle$ associated with pth electronic state $|\phi_p\rangle$. These wavepackets are then multiplied by their respective electronic states and linearly combined to reconstruct the full wave function (Figure 1c). This structure allows each PQC to better adapt to its corresponding wavepacket, resulting in a more compact and efficient ansatz.

The nonadiabatic Hamiltonian in the diabatic representation can be generally expressed as

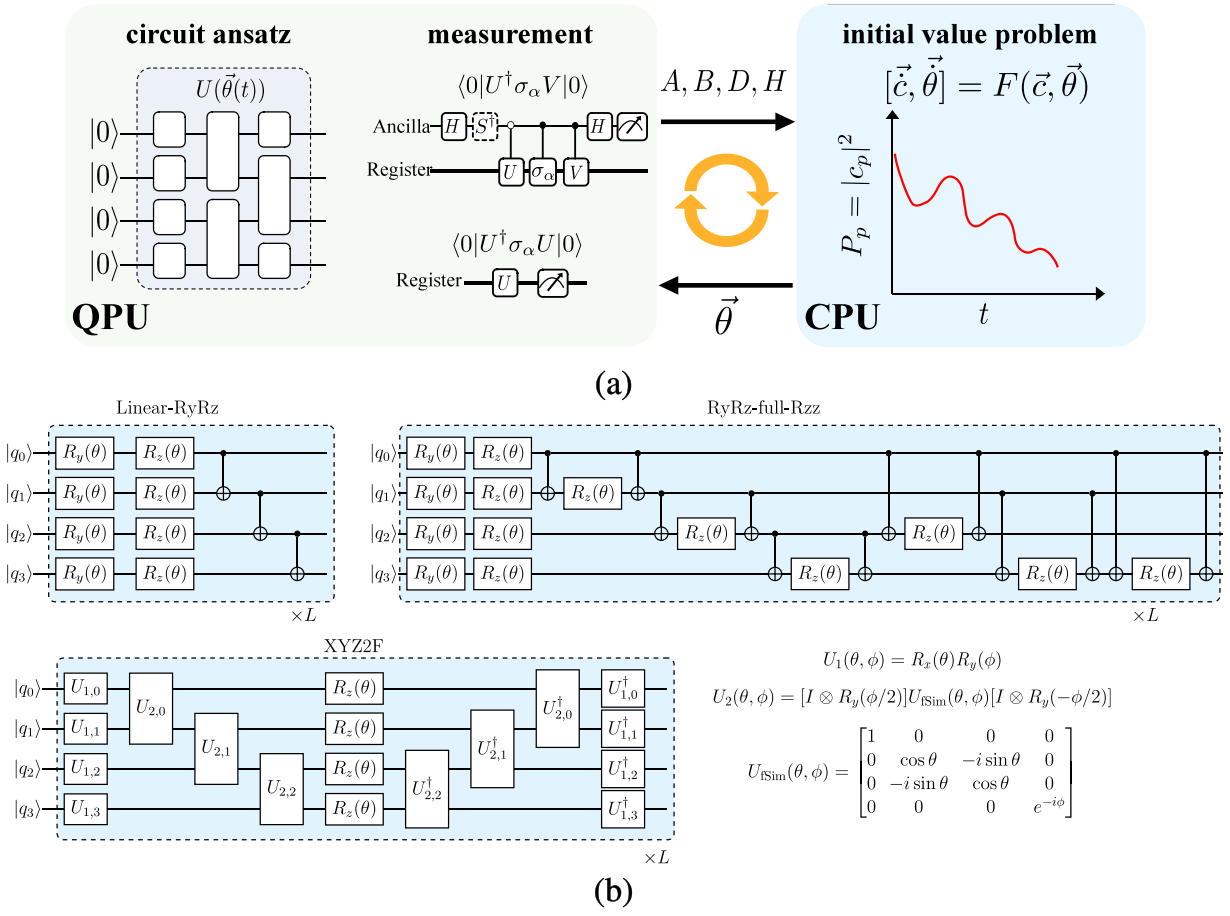

Figure 2. (a) Workflow of the hybrid quantum–classical multiset variational quantum dynamics algorithm. The quantum computer prepares the nuclear wavepacket and measures the matrix elements using direct measurement or the Hadamard test algorithm. The classical computer updates the parameters by solving an initial value problem. (b) Three types of ansatzes used in this study: linear-RyRz ansatz, RyRz-full-Rzz ansatz, and XYZ2F ansatz.

https://doi.org/10.1021/acs.jpclett.5c00739
J. Phys. Chem. Lett. 2025, 16, 3911–3919

$$\hat{H} = \hat{T} + \begin{bmatrix} \hat{V}_{11} & \hat{V}_{12} & \cdots & \hat{V}_{1N} \\ \hat{V}_{21} & \hat{V}_{22} & \cdots & \hat{V}_{2N} \\ \cdots & \cdots & \cdots & \cdots \\ \hat{V}_{N1} & \hat{V}_{N2} & \cdots & \hat{V}_{NN} \end{bmatrix} \tag{4}$$

The diabatic energies and coupling terms depend on nuclear coordinates $\hat{V}_{pq} \equiv \hat{V}_{pq}(\vec{R})$.

Based on the McLachlan's time-dependent variational principle $\delta\|(\hat{H} - i\partial/\partial t)|\Psi(\vec{\theta}(t))\rangle\|^2 = 0$,[65] the equations of motion of the MS-VQD are

$$\sum_k |c_p|^2 \mathrm{Re}(A_{lk}^{pp} - D_l^{pp} D_k^{pp*}) \dot{\theta}_k^p = \mathrm{Im} \sum_q c_p^* c_q (B_l^{pq} - H_{pq} D_l^{pp}) \tag{5}$$

$$\dot{c}_p + c_p \sum_k D_k^{pp*} \dot{\theta}_k^p + i \sum_q c_q H_{pq} = 0 \tag{6}$$

where matrices **A**, **B**, **D**, and **H** are

$$A_{lk}^{pp} = \left\langle \frac{\partial \chi_p}{\partial \theta_l^p} \middle| \frac{\partial \chi_p}{\partial \theta_k^p} \right\rangle \tag{7}$$

$$B_l^{pq} = \left\langle \frac{\partial \chi_p}{\partial \theta_l^p} \middle| \hat{T} + \hat{V}_{pq} \middle| \chi_q \right\rangle \tag{8}$$

$$D_k^{pp} = \left\langle \frac{\partial \chi_p}{\partial \theta_k^p} \middle| \chi_p \right\rangle \tag{9}$$

$$H_{pq} = \langle \chi_p | \hat{T} + \hat{V}_{pq} | \chi_q \rangle \tag{10}$$

The detailed derivation is provided in the Appendix. The matrix elements of **A**, **B**, **D**, and **H** can be measured using either the direct measurement or the Hadamard test algorithm, as illustrated in Figure 2a. The details are presented in section 1 and Figure S1 of the Supporting Information (SI). When only a single electronic state is present, eqs 5 and 6 are reduced to simplified forms

$$\sum_k \mathrm{Re}(A_{lk} - D_l D_k^*) \dot{\theta}_k = \mathrm{Im}(B_l - E D_l) \tag{11}$$

$$\dot{c} + c \sum_k D_k \dot{\theta}_k + icE = 0 \tag{12}$$

Equation 11 is consistent with the equation of motion for the traditional VQD, as derived in the previous studies.[27] At first glance, the MS-VQD appears more complex than the VQD due to the additional index p, which corresponds to a specific electronic state. However, the left-hand side of eq 5 depends only on p, resulting in a block-diagonal structure. This simplifies solving the linear equation on a classical computer. A discussion of the classical overhead of solving linear equations is given in section 2 of the SI.

The overall processes of the MS-VQD are illustrated in Figure 2a and include the following:

(i) Initialize $\vec{c}$ and $\vec{\theta}$ according to the initial condition;

(ii) Prepare the PQC on a quantum computer and measure the matrix elements of **A**, **B**, **D**, and **H**;

(iii) Calculate time derivative $\dot{\vec{\theta}}$ and $\dot{\vec{c}}$ according to eqs 5 and 6 and update $\vec{\theta}$ and $\vec{c}$ with any proper solver for initial value problems on a classical computer. Return to (ii).

To evaluate the effectiveness of the MS-VQD in simulating nonadiabatic quantum dynamics, we applied it to model the excitation energy transfer dynamics in one-dimensional molecular aggregates using the Frenkel–Holstein model Hamiltonian, which is

$$\hat{H} = \sum_p \varepsilon_p |\phi_p\rangle\langle\phi_p| + \sum_p J\left(|\phi_p\rangle\langle\phi_{p+1}| + |\phi_{p+1}\rangle\langle\phi_p|\right) + \sum_{pm} \omega_m \hat{b}_{pm}^\dagger \hat{b}_{pm} + \sum_{pm} g_m \omega_m |\phi_p\rangle\langle\phi_p| (\hat{b}_{pm}^\dagger + \hat{b}_{pm}) \tag{13}$$

In this model, ε_p denotes the excitation energy of local electronic state $|\phi_p\rangle$, J denotes the excitonic coupling, and $\hat{b}_{pm}^\dagger$ and $\hat{b}_{pm}$ correspond to the creation and annihilation operators of the mth vibrational mode of the pth molecule, respectively, with frequency ω_m and dimensionless electron–vibration coupling constant g_m.

To encode the infinitely large bosonic Hilbert space into qubits, we truncated the local bosonic energy levels to a finite size d and mapped them to qubit states using the Gray code. For example, when $d = 4$, the encoding follows $|00\rangle \rightarrow |0\rangle$, $|01\rangle \rightarrow |1\rangle$, $|11\rangle \rightarrow |2\rangle$, and $|10\rangle \rightarrow |3\rangle$. The Gray code has been shown to reduce not only the number of qubits compared to unary encoding but also the number of two-qubit gates needed to represent $b^\dagger/b$ compared to standard binary encoding.[66] In addition, the MS-VQD is also compatible with the recently proposed variational encoding method, which can further reduce qubit requirements.[67] Besides encoding the bosonic state, in the traditional VQD, electronic states are encoded using the binary code. For a system with N molecules and K nuclear degrees of freedom per molecule, since the MS-VQD does not explicitly encode electronic states on the quantum computer, the number of qubits is reduced from $NK \log_2 d + \log_2 N$ in the VQD to $NK \log_2 d$. Meanwhile, the number of Hamiltonian terms after mapping into qubits in MS-VQD is also much smaller than that in the VQD shown in Figure S3.

In the choice of ansatz for each PQC in both the VQD and the MS-VQD, any proper ansatz can be used. We employed three types: the linear-RyRz ansatz,[58] the RyRz-full-Rzz ansatz, and the XYZ2F ansatz,[62] as shown in Figure 2b. The first two are simple hardware-efficient ansatzes, where single-qubit rotation gates and two-qubit CNOT/Rzz gates are placed in alternation. The third, XYZ2F, is a recently developed ansatz[62] that satisfies key physical constraints and has been proven to be universal, systematically improvable, and size-consistent. In our calculations, the number of layers (L) of these ansatzes is gradually increased to enhance the expressivity.

We primarily focused on exciton population dynamics, defined as $P_p(t) = |\langle\phi_p|\Psi(t)\rangle|^2$. The initial condition assumes that the exciton is localized on the first molecule, with all vibrational modes in their ground state. In the MS-VQD, $P_p = |c_p|^2$, which can be directly computed classically, whereas in the VQD, P_p is obtained by sampling the qubits encoding the electronic state, expressed as $P(j_1 j_2 \ldots, p = \sum_k j_k 2^k)$. All simulations were performed without noise using the quantum simulator TensorCircuit[68] and TenCirChem.[69] Reference data were calculated using the numerically exact time-dependent density matrix renormalization group algorithm (TD-DMRG).[14] A discussion about the impact of noise on the

https://doi.org/10.1021/acs.jpclett.5c00739
J. Phys. Chem. Lett. 2025, 16, 3911−3919

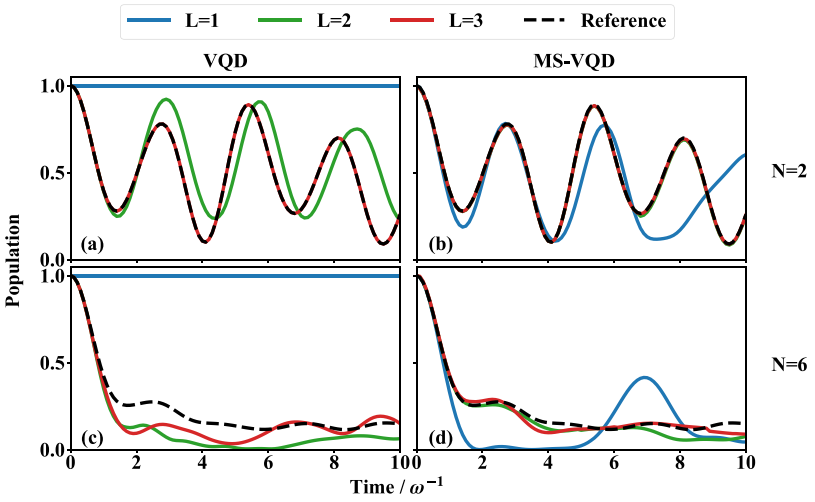

Figure 3. Exciton population on the first molecule as a function of time, $|\langle\phi_1|\Psi(t)\rangle|^2$. Results of (a) the VQD and (b) the MS-VQD for the dimer model. Different colors represent different layers of the ansatz, with L = 1, 2, or 3. The dashed black curve shows the reference results calculated by the time-dependent density matrix renormalization group algorithm. (c and d) Similar to panels a and b, respectively, but for the hexamer model. The linear-RyRz ansatz is used.

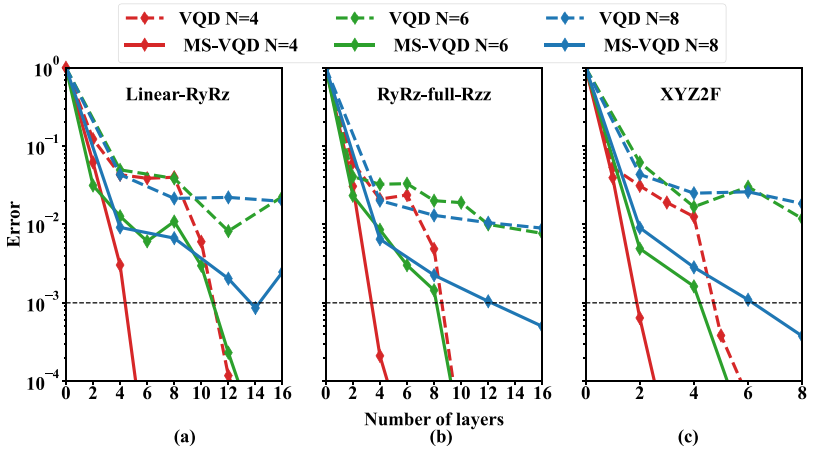

Figure 4. Population errors for different layers of an ansatz in the VQD and MS-VQD: (a) linear-RyRz ansatz, (b) RyRz-full-Rzz ansatz, and (c) XYZ2F ansatz. Different colors represent different system sizes.

simulated results and the resource requirements of error mitigation are provided in section 4 of the SI.

Figure 3 presents exciton population P_1 of the first molecule for a dimer (N = 2) and a hexamer (N = 6), using the linear-RyRz ansatz with one to three layers. One vibrational mode per molecule is considered. The following parameters are used: g = 1, J = −1, d = 2, and dt = 0.1, with ω = 1 as the unit. Comparing panel a of Figure 3 to panel c and panel b to panel d, we observed that as the number of molecules increases, the simulation becomes more challenging, requiring additional ansatz layers to maintain accuracy for both the VQD and the MS-VQD. Compared to the VQD, the MS-VQD consistently achieves a higher accuracy with the same L, regardless of system size. Similar behaviors were observed for the other two ansatzes, as shown in Figures S6 and S7.

To quantitatively assess the performance of the MS-VQD and VQD across different system sizes, we defined the population error as

$$\varepsilon = \frac{\sum_{k=1}^{N_{\text{steps}}} |P_1(t_k) - P_1^{\text{ref}}(t_k)|}{N_{\text{steps}}};\ t \in [0,\ 10/\omega] \tag{14}$$

Panels a−c of Figure 4 illustrate how the error evolves with an increasing number of ansatz layers L for the three different ansatzes (the error at L = 0 is arbitrarily set to 1 to guide the eye). Regardless of the ansatz used, the MS-VQD exhibits faster convergence with L compared to the VQD. For example, in the case of an octamer using the linear-RyRz ansatz, the MS-VQD with L = 4 achieves higher accuracy than the VQD with L = 16. Similar trends are observed for the RyRz-full-Rzz and XYZ2F ansatzes, suggesting that the advantage of the MS-VQD is likely to be generalizable across other ansatz choices. When the three ansatzes within the MS-VQD are compared, the RyRz-full-Rzz ansatz performs slightly better than the linear-RyRz ansatz in terms of PQC layers. For the octamer with L = 16, the error of the RyRz-full-Rzz ansatz is 5.0×10^{-4}, while that of the linear-RyRz ansatz is 2.0×10^{-3}. The XYZ2F ansatz performs much better, achieving an error of 3.8×10^{-4} with only L = 8. This trend is consistent with the findings from ground state calculations.[62] We also used the wave function infidelity $1 - \text{Re}\langle\Psi^{\text{ref}}(t)|\Psi(t)\rangle$ as the error metric, and the findings are similar as shown in Figure S8.

Figure 5a summarizes the number of layers L required to achieve a population error of less than 10^{-3} for different system

https://doi.org/10.1021/acs.jpclett.5c00739
J. Phys. Chem. Lett. 2025, 16, 3911−3919

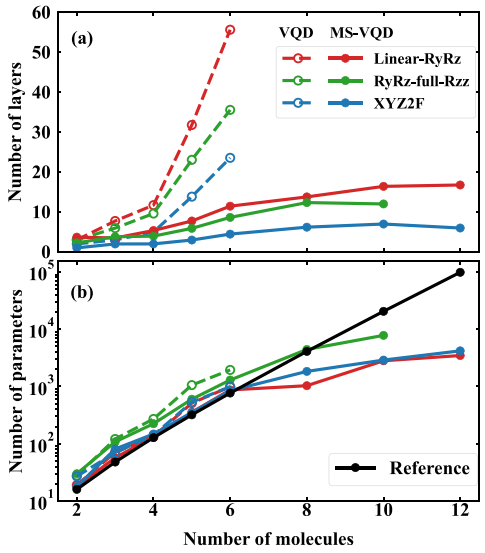

Figure 5. (a) Required number of ansatz layers L and (b) required number of parameters for different system sizes to achieve an error of less than 10^{-3}. Solid lines represent MS-VQD results, while dashed lines represent VQD results. Different colors correspond to different ansatzes. In panel b, the black solid line represents the full Hilbert space dimension.

sizes. As the system size increases, the VQD struggles to maintain accuracy, requiring a rapidly increasing number of layers. In contrast, the MS-VQD scales much more favorably, requiring many fewer layers to achieve the same accuracy. This trend is consistent across all three ansatzes, further highlighting the superiority of the MS-VQD for nonadiabatic dynamics involving a large number of electronic states. Regarding the number of parameters in the ansatzes shown in Figure 5b, for system sizes smaller than a hexamer, the number of parameters in the MS-VQD slightly exceeds the full Hilbert space dimension, indicating some redundancy in parametrization. However, for systems larger than a hexamer, the number of parameters becomes smaller than the full Hilbert space dimension, with a much slower scaling than the exponential. This suggests that the MS-VQD has the potential to surpass the exact classical algorithm for large systems (see more discussion in section 7 of the SI). When comparing the MS-VQD to state-of-the-art approximate but "numerically exact" classical methods, such as multilayer multiconfiguration time-dependent Hartree (ML-MCTDH)[12] and TD-DMRG,[14] further investigation is required to determine whether the MS-VQD can outperform these approaches in practical applications. Compared to the VQD, the MS-VQD requires slightly fewer parameters for system sizes smaller than a hexamer (the classical simulations of VQD for system sizes larger than a hexamer exceeded our available computational resources). This suggests that the MS-VQD can achieve the same accuracy with an ansatz depth slightly shorter than $1/N$ of that required by the VQD. This finding aligns with the schematic diagram in Figure 1, illustrating that the VQD requires N ansatz blocks to accurately capture the dynamics of N electronic states accurately.

Due to the exponentially large computational cost of classical simulations of quantum computing, the above calculations for large molecular aggregates are restricted to local bosonic levels $d = 2$. However, this truncation is not sufficient to accurately represent real molecular aggregates. Therefore, we evaluated the performance of the VQD and MS-VQD with different d values on a molecular dimer. After mapping the Hamiltonian to qubits, the total number of terms increases linearly with d (Figure S3a), indicating that a larger d will result in a more entangled state and thus a deeper PQC. Since the MS-VQD involves fewer Hamiltonian terms than the VQD, it is expected that the MS-VQD requires a shallower PQC. As shown in Figure 6, as d increases, the number of

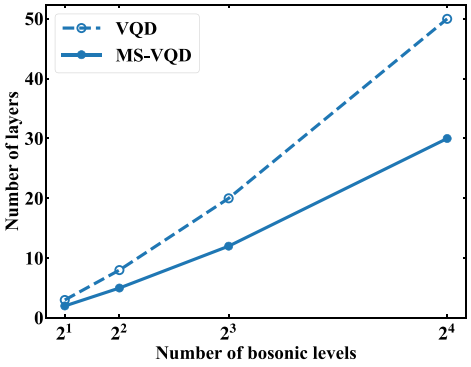

Figure 6. Required number of ansatz layers to achieve an error of less than 10^{-3} for different numbers of local bosonic levels d.

ansatz layers required for the MS-VQD to achieve an error of less than 10^{-3} increases much more slowly compared to the VQD. This suggests that the MS-VQD maintains its computational advantage even with a large local bosonic space.

Furthermore, we examined the robustness of the MS-VQD across different coupling regimes and varying numbers of vibrational modes, as detailed in section 8 of the SI. Figures S9 and S10 demonstrate that the advantage of the MS-VQD over the VQD remains robust across different electronic and electron−vibration coupling strengths as well as for multiple numbers of vibrational modes.

Finally, we analyzed the computational cost of the VQD and MS-VQD. The scaling of circuit depth and the number of measurements with respect to the number of ansatz layers L and the number of parameters n_θ are summarized in Table 1. N

Table 1. Circuit Depths and Numbers of Measurements Required to Calculate Matrices A, B, D, and H

algorithm		A_{lk}^{pp}	D_k^{pp}	B_l^{pq}	H_{pq}
VQD	depth	$O(L)$	$O(L)$	$O(L)$	$O(L)$
	times	$O(n_\theta^2)$	$O(n_\theta)$	$O(fn_\theta)$	$O(f)$
MS-VQD	depth	$O(L/N)$	$O(L/N)$	$O(\beta L/N)$	$O(\beta L/N)$
	times	$O(n_\theta^2/N)$	$O(n_\theta)$	$O(fn_\theta/N)$	$O(f)$

is the number of electronic states. For the VQD, using either direct measurement or the Hadamard test algorithm, the circuit depth required to compute A_{lk}, D_k, B_l, and E is $O(L)$. The corresponding number of measurements required is $O(n_\theta^2)$, $O(n_\theta)$, $O(fn_\theta)$, and $O(f)$, respectively, where f is the number of Hamiltonian terms after mapping to qubits. In comparison, assuming that the number of parameters in the MS-VQD is the same as that in the VQD to achieve the same accuracy, the number ansatz layers required for the MS-VQD is $1/N$ of that for the VQD. Hence, the circuit depth required to measure electronic diagonal elements A_{lk}^{pp} and D_k^p in the MS-VQD is both $O(L/N)$. However, for electronic nondiagonal

https://doi.org/10.1021/acs.jpclett.5c00739
J. Phys. Chem. Lett. 2025, 16, 3911−3919

elements B_l^{pq} and H_{pq}, all gates with parameters must be controlled by an ancilla qubit in the Hadamard test, introducing an overhead prefactor β. For example, a controlled-Ry gate can be decomposed into two Ry gates and two CNOT gates, giving $\beta = 4$. This results in a circuit depth of $O(\beta L/N)$. The number of measurements required to obtain A_{lk}^{pp} and D_k^p is $O((n_\theta/N)^2 \times N) = O(n_\theta^2/N)$ and $O(n_\theta/N \times N) = O(n_\theta)$, respectively. The number of measurements required for H_{pq} seems to be $O(fN^2)$, but since only subset $\hat{T} + \hat{V}_{pq}$ of whole Hamiltonian $\hat{H}$ needs to be measured for each pq pair, the overall cost remains $O(f)$. A similar argument applies to B_l^{pq}, which requires $O(fn_\theta/N)$ measurements. Thus, while the equation of motion of the MS-VQD seems more complex than that of the VQD, both the circuit depth and the number of measurements of some matrix elements benefit from a $1/N$ reduction. This advantage becomes particularly useful as the number of electronic states increases.

In this Letter, we propose a novel multiset variational quantum dynamics algorithm for simulating nonadiabatic quantum dynamics and derive the equations of motion within the framework of McLachlan's time-dependent variational principle for the first time. This is the main contribution of our work. The MS-VQD algorithm utilizes a set of parametrized quantum circuits to represent the entire electronic−nuclear coupled wave function, where each PQC corresponds to the wavepacket on a single potential energy surface. This structure allows the ansatz to better adapt to the landscape of different PESs, making the PQCs more compact. Through simulations of the Frenkel−Holstein electron−vibration coupling model, we found that the ansatz depth required by the MS-VQD is approximately reduced to $1/N$ of that in the VQD while maintaining the same accuracy. This reduction in quantum resource requirements makes the MS-VQD more suitable for implementation on noisy quantum computers. Moreover, the advantage of the MS-VQD over the VQD is robust across different ansatz choices, sizes of the local bosonic space, coupling regimes, and numbers of vibrational modes. In the future, the MS-VQD can also be extended to imaginary-time evolution[70] for calculating quantum statistical properties. Additionally, it can be combined with grid basis to study nonadiabatic dynamics on real anharmonic potential energy surfaces.[34,71] Despite its advantages, some challenges remain. Although the MS-VQD outperforms the VQD in simulating nonadiabatic dynamics, achieving highly accurate results still requires a large number of parameters. For large molecular aggregates that may exhibit a quantum advantage, the quantum resources required by all three hardware-efficient ansatzes explored in this study have exceeded the capabilities of current noisy quantum computers. Given the MS-VQD's strength in adapting to wavepackets on each PES, exploring an independent and adaptive ansatz[57,72,73] for each PQC to replace the shared and fixed ansatz may further compact the circuit and enhance efficiency.

APPENDIX: DERIVATION OF THE MS-VQD

Let any vector on the tangent space of $|\Psi(\vec{\theta}(t))\rangle$ be denoted as φ. According to McLachlan's time-dependent variational principle, the optimal solution for $\dot{\Psi}(\vec{\theta}(t))$ is vector φ that minimizes functional $\mathcal{F}$

$$\mathcal{F} = \|\varphi + i\hat{H}\Psi(\vec{\theta}(t))\|^2 \tag{15}$$

The minimal point satisfies

$$\delta\mathcal{F} = \langle\delta\varphi|\dot{\Psi}(\vec{\theta}(t)) + i\hat{H}\Psi(\vec{\theta}(t))\rangle + \text{h.c.} = 0 \tag{16}$$

For the multiset wave function ansatz

$$\dot{\Psi}(\vec{\theta}(t)) = \sum_q \dot{c}_q\phi_q\chi_q + \sum_{qk} c_q\phi_q\frac{\partial\chi_q}{\partial\theta_k^q}\dot{\theta}_k^q \tag{17}$$

$$\delta\varphi = \sum_p \delta a_p\phi_p\chi_p + \sum_{pl} c_p\phi_p\frac{\partial\chi_p}{\partial\theta_l^p}\delta b_l^p \tag{18}$$

Note that while δa_p can be complex, δb_l^p must be real, as required by the quantum computer. Substituting eqs 17 and 18 into eq 16, we obtain

$$\left\langle \sum_p \delta a_p\phi_p\chi_p + \sum_{pl} c_p\phi_p\frac{\partial\chi_p}{\partial\theta_l^p}\delta b_l^p \middle| \sum_q \dot{c}_q\phi_q\chi_q + \sum_{qk} c_q\phi_q\frac{\partial\chi_q}{\partial\theta_k^q}\dot{\theta}_k^q + i\hat{H}\sum_q c_q\phi_q\chi_q \right\rangle + \text{h.c.} = 0 \tag{19}$$

The above formula can be separated into three parts: δa_p, δa_p^* (since δa_p is complex, δa_p and δa_p^* can be treated as independent variations), and δb_l^p. Using the relation $\langle\phi_p|\phi_q\rangle = \delta_{pq}$, these three parts are given by the following.

1. δa_p part:

$$\dot{c}_p + c_p\sum_k D_k^{pp^*}\dot{\theta}_k^p + i\sum_q c_q H_{pq} = 0 \tag{20}$$

2. δa_p^* part:

$$\dot{c}_p^* + c_p^*\sum_k D_k^{pp}\dot{\theta}_k^p - i\sum_q c_q^* H_{pq}^* = 0 \tag{21}$$

Comparing eqs 20 and 21, we see that if one expression holds, the other must also be valid. Therefore, it is sufficient to consider only one of them.

3. δb_l^p part:

$$c_p^*\left\langle\frac{\partial\chi_p}{\partial\theta_l^p}\middle|\dot{c}_p\chi_p\right\rangle + c_p^*\left\langle\frac{\partial\chi_p}{\partial\theta_l^p}\middle|\sum_k c_p\frac{\partial\chi_p}{\partial\theta_k^p}\dot{\theta}_k^p\right\rangle + c_p^*\left\langle\frac{\partial\chi_p}{\partial\theta_l^p}\middle|i\sum_q(\hat{T}+\hat{V}_{pq})c_q\chi_q\right\rangle + \text{h.c.} = 0 \tag{22}$$

Substituting $\dot{c}_p$ from eq 20 into eq 22, we obtain eq 5.

ASSOCIATED CONTENT

Supporting Information

The Supporting Information is available free of charge at https://pubs.acs.org/doi/10.1021/acs.jpclett.5c00739.

Circuits to measure matrix elements in the MS-VQD, classical overhead of solving linear equations, number of Hamiltonian terms after mapping to qubits, impact of noise, population dynamics with the RyRz-full-Rzz ansatz and XYZ2F ansatz, infidelity as a function of the number of ansatz layers, scaling of the classical exact

https://doi.org/10.1021/acs.jpclett.5c00739
J. Phys. Chem. Lett. 2025, 16, 3911−3919

algorithm, and performance of the MS-VQD and VQD with different coupling strengths and numbers of modes (PDF)

AUTHOR INFORMATION

Corresponding Author

Jiajun Ren − *Key Laboratory of Theoretical and Computational Photochemistry, Ministry of Education, College of Chemistry, Beijing Normal University, Beijing 100875, People's Republic of China;* orcid.org/0000-0002-1508-4943; Email: jjren@bnu.edu.cn

Authors

Jingjing Li − *Key Laboratory of Theoretical and Computational Photochemistry, Ministry of Education, College of Chemistry, Beijing Normal University, Beijing 100875, People's Republic of China*

Weitang Li − *School of Science and Engineering, The Chinese University of Hong Kong, Shenzhen 518172, P. R. China*

Xiaoxiao Xiao − *Key Laboratory of Theoretical and Computational Photochemistry, Ministry of Education, College of Chemistry, Beijing Normal University, Beijing 100875, People's Republic of China*

Limin Liu − *Key Laboratory of Theoretical and Computational Photochemistry, Ministry of Education, College of Chemistry, Beijing Normal University, Beijing 100875, People's Republic of China*

Zhendong Li − *Key Laboratory of Theoretical and Computational Photochemistry, Ministry of Education, College of Chemistry, Beijing Normal University, Beijing 100875, People's Republic of China;* orcid.org/0000-0002-0683-6293

Weihai Fang − *Key Laboratory of Theoretical and Computational Photochemistry, Ministry of Education, College of Chemistry, Beijing Normal University, Beijing 100875, People's Republic of China;* orcid.org/0000-0002-1668-465X

Complete contact information is available at: https://pubs.acs.org/10.1021/acs.jpclett.5c00739

Notes

The authors declare no competing financial interest.

ACKNOWLEDGMENTS

This work is supported by the Innovation Program for Quantum Science and Technology (Grant 2023ZD0300200), the NSAF (Grant U2330201), the National Natural Science Foundation of China (Grants 22422301 and 22273005), and the Fundamental Research Funds for the Central Universities.

REFERENCES

(1) Yarkony, D. R. Nonadiabatic Quantum Chemistry- Past, Present, and Future. *Chem. Rev.* **2012**, *112*, 481−498.

(2) Long, R.; Prezhdo, O. V.; Fang, W. Nonadiabatic charge dynamics in novel solar cell materials. *Wiley Interdiscip. Rev.: Comput. Mol. Sci.* **2017**, *7*, e1305.

(3) Jang, S. J.; Mennucci, B. Delocalized excitons in natural light-harvesting complexes. *Rev. Mod. Phys.* **2018**, *90*, 035003.

(4) Dimitriev, O. P. Dynamics of excitons in conjugated molecules and organic semiconductor systems. *Chem. Rev.* **2022**, *122*, 8487−8593.

(5) Brédas, J.-L.; Sargent, E. H.; Scholes, G. D. Photovoltaic concepts inspired by coherence effects in photosynthetic systems. *Nat. Mater.* **2017**, *16*, 35−44.

(6) Wang, L.; Allodi, M. A.; Engel, G. S. Quantum coherences reveal excited-state dynamics in biophysical systems. *Nat. Rev. Chem.* **2019**, *3*, 477−490.

(7) Schultz, J. D.; Yuly, J. L.; Arsenault, E. A.; Parker, K.; Chowdhury, S. N.; Dani, R.; Kundu, S.; Nuomin, H.; Zhang, Z.; Valdiviezo, J.; et al. Coherence in Chemistry: Foundations and Frontiers. *Chem. Rev.* **2024**, *124*, 11641−11766.

(8) Tully, J. C. Perspective: Nonadiabatic dynamics theory. *J. Chem. Phys.* **2012**, *137*, 22A301.

(9) Curchod, B. F.; Martínez, T. J. Ab initio nonadiabatic quantum molecular dynamics. *Chem. Rev.* **2018**, *118*, 3305−3336.

(10) Makri, N. Quantum dissipative dynamics: A numerically exact methodology. *J. Phys. Chem. A* **1998**, *102*, 4414−4427.

(11) Worth, G. A.; Meyer, H.-D.; Köppel, H.; Cederbaum, L.; Burghardt, I. Using the MCTDH wavepacket propagation method to describe multimode non-adiabatic dynamics. *Int. Rev. Phys. Chem.* **2008**, *27*, 569−606.

(12) Wang, H.; Thoss, M. Multilayer formulation of the multi-configuration time-dependent Hartree theory. *J. Chem. Phys.* **2003**, *119*, 1289−1299.

(13) Tanimura, Y. Numerically "exact" approach to open quantum dynamics: The hierarchical equations of motion (HEOM). *J. Chem. Phys.* **2020**, *153*, 020901.

(14) Ren, J.; Li, W.; Jiang, T.; Wang, Y.; Shuai, Z. Time-dependent density matrix renormalization group method for quantum dynamics in complex systems. *Wiley Interdiscip. Rev.: Comput. Mol. Sci.* **2022**, *12*, e1614.

(15) Cao, Y.; Romero, J.; Olson, J. P.; Degroote, M.; Johnson, P. D.; Kieferová, M.; Kivlichan, I. D.; Menke, T.; Peropadre, B.; Sawaya, N. P.; et al. Quantum chemistry in the age of quantum computing. *Chem. Rev.* **2019**, *119*, 10856−10915.

(16) Bauer, B.; Bravyi, S.; Motta, M.; Chan, G. K.-L. Quantum algorithms for quantum chemistry and quantum materials science. *Chem. Rev.* **2020**, *120*, 12685−12717.

(17) McArdle, S.; Endo, S.; Aspuru-Guzik, A.; Benjamin, S. C.; Yuan, X. Quantum computational chemistry. *Rev. Mod. Phys.* **2020**, *92*, 015003.

(18) Ollitrault, P. J.; Miessen, A.; Tavernelli, I. Molecular quantum dynamics: A quantum computing perspective. *Acc. Chem. Res.* **2021**, *54*, 4229−4238.

(19) Motta, M.; Rice, J. E. Emerging quantum computing algorithms for quantum chemistry. *Wiley Interdiscip. Rev.: Comput. Mol. Sci.* **2022**, *12*, e1580.

(20) Delgado-Granados, L. H.; Krogmeier, T. J.; Sager-Smith, L. M.; Avdic, I.; Hu, Z.; Sajjan, M.; Abbasi, M.; Smart, S. E.; Narang, P.; Kais, S.; et al. Quantum Algorithms and Applications for Open Quantum Systems. *Chem. Rev.* **2025**, *125*, 1823−1839.

(21) Fauseweh, B. Quantum many-body simulations on digital quantum computers: State-of-the-art and future challenges. *Nat. Commun.* **2024**, *15*, 2123.

(22) Lloyd, S. Universal quantum simulators. *Science* **1996**, *273*, 1073−1078.

(23) Miessen, A.; Ollitrault, P. J.; Tacchino, F.; Tavernelli, I. Quantum algorithms for quantum dynamics. *Nat. Comput. Sci.* **2023**, *3*, 25−37.

(24) Childs, A. M.; Wiebe, N. Hamiltonian simulation using linear combinations of unitary operations. *Quantum Inf. Comput.* **2012**, *12*, 901−924.

(25) Berry, D. W.; Childs, A. M.; Cleve, R.; Kothari, R.; Somma, R. D. Simulating Hamiltonian dynamics with a truncated Taylor series. *Phys. Rev. Lett.* **2015**, *114*, 090502.

(26) Li, Y.; Benjamin, S. C. Efficient variational quantum simulator incorporating active error minimization. *Phys. Rev. X* **2017**, *7*, 021050.

(27) Yuan, X.; Endo, S.; Zhao, Q.; Li, Y.; Benjamin, S. C. Theory of variational quantum simulation. *Quantum* **2019**, *3*, 191.

(28) Campbell, E. Random compiler for fast Hamiltonian simulation. *Phys. Rev. Lett.* **2019**, *123*, 070503.
(29) Cirstoiu, C.; Holmes, Z.; Iosue, J.; Cincio, L.; Coles, P. J.; Sornborger, A. Variational fast forwarding for quantum simulation beyond the coherence time. *npj Quantum Information* **2020**, *6*, 82.
(30) Hu, Z.; Xia, R.; Kais, S. A quantum algorithm for evolving open quantum dynamics on quantum computing devices. *Sci. Rep.* **2020**, *10*, 3301.
(31) Barison, S.; Vicentini, F.; Carleo, G. An efficient quantum algorithm for the time evolution of parameterized circuits. *Quantum* **2021**, *5*, 512.
(32) Schlimgen, A. W.; Head-Marsden, K.; Sager, L. M.; Narang, P.; Mazziotti, D. A. Quantum simulation of the Lindblad equation using a unitary decomposition of operators. *Phys. Rev. Res.* **2022**, *4*, 023216.
(33) Wan, L.; Liu, J.; Li, Z.; Yang, J. Hybrid Hamiltonian Simulation for Excitation Dynamics. *J. Phys. Chem. Lett.* **2024**, *15*, 11234−11243.
(34) Kassal, I.; Jordan, S. P.; Love, P. J.; Mohseni, M.; Aspuru-Guzik, A. Polynomial-time quantum algorithm for the simulation of chemical dynamics. *Proc. Natl. Acad. Sci. U. S. A.* **2008**, *105*, 18681−18686.
(35) Macridin, A.; Spentzouris, P.; Amundson, J.; Harnik, R. Electron-phonon systems on a universal quantum computer. *Phys. Rev. Lett.* **2018**, *121*, 110504.
(36) Endo, S.; Sun, J.; Li, Y.; Benjamin, S. C.; Yuan, X. Variational quantum simulation of general processes. *Phys. Rev. Lett.* **2020**, *125*, 010501.
(37) Ollitrault, P. J.; Mazzola, G.; Tavernelli, I. Nonadiabatic molecular quantum dynamics with quantum computers. *Phys. Rev. Lett.* **2020**, *125*, 260511.
(38) Lee, C.-K.; Zhong Lau, J. W.; Shi, L.; Kwek, L. C. Simulating energy transfer in molecular systems with digital quantum computers. *J. Chem. Theory Comput.* **2022**, *18*, 1347−1358.
(39) Tazhigulov, R. N.; Sun, S.-N.; Haghshenas, R.; Zhai, H.; Tan, A. T.; Rubin, N. C.; Babbush, R.; Minnich, A. J.; Chan, G. K.-L. Simulating models of challenging correlated molecules and materials on the sycamore quantum processor. *PRX Quantum* **2022**, *3*, 040318.
(40) Kovyrshin, A.; Skogh, M.; Tornberg, L.; Broo, A.; Mensa, S.; Sahin, E.; Symons, B. C.; Crain, J.; Tavernelli, I. Nonadiabatic nuclear-electron dynamics: a quantum computing approach. *J. Phys. Chem. Lett.* **2023**, *14*, 7065−7072.
(41) Zhang, Y.; Hu, Z.; Wang, Y.; Kais, S. Quantum simulation of the radical pair dynamics of the avian compass. *J. Phys. Chem. Lett.* **2023**, *14*, 832−837.
(42) Gomes, N.; Williams-Young, D. B.; de Jong, W. A. Computing the Many-Body green's function with adaptive variational quantum dynamics. *J. Chem. Theory Comput.* **2023**, *19*, 3313−3323.
(43) Luo, J.; Lin, K.; Gao, X. Variational quantum simulation of lindblad dynamics via quantum state diffusion. *J. Phys. Chem. Lett.* **2024**, *15*, 3516−3522.
(44) Li, X.; Lyu, S.-X.; Wang, Y.; Xu, R.-X.; Zheng, X.; Yan, Y. Toward quantum simulation of non-Markovian open quantum dynamics: A universal and compact theory. *Phys. Rev. A* **2024**, *110*, 032620.
(45) Lan, Z.; Liang, W. Integrating Self-Initialized Local Thermalizing Lindblad Operators for Variational Quantum Algorithm with Quantum Jump: Implementation and Performance. *J. Chem. Theory Comput.* **2024**, *20*, 10317−10327.
(46) Lyu, N.; Khazaei, P.; Geva, E.; Batista, V. S. Simulating Cavity-Modified Electron Transfer Dynamics on NISQ Computers. *J. Phys. Chem. Lett.* **2024**, *15*, 9535−9542.
(47) Gallina, F.; Bruschi, M.; Cacciari, R.; Fresch, B. Simulating Non-Markovian Dynamics in Multidimensional Electronic Spectroscopy via Quantum Algorithm. *J. Chem. Theory Comput.* **2024**, *20*, 10588−10601.
(48) Walters, P. L.; Sherazi, M. U.; Wang, F. Variational Quantum Algorithm for Non-Markovian Quantum Dynamics Using an Ensemble of Ehrenfest Trajectories. *J. Phys. Chem. Lett.* **2025**, *16*, 1001−1006.
(49) Dan, X.; Geva, E.; Batista, V. S. Simulating Non-Markovian Quantum Dynamics on NISQ Computers Using the Hierarchical Equations of Motion. *J. Chem. Theory Comput.* **2025**, *21*, 1530−1546.
(50) Chen, M.-C.; Gong, M.; Xu, X.; Yuan, X.; Wang, J.-W.; Wang, C.; Ying, C.; Lin, J.; Xu, Y.; Wu, Y.; et al. Demonstration of adiabatic variational quantum computing with a superconducting quantum coprocessor. *Phys. Rev. Lett.* **2020**, *125*, 180501.
(51) Cerezo, M.; Arrasmith, A.; Babbush, R.; Benjamin, S. C.; Endo, S.; Fujii, K.; McClean, J. R.; Mitarai, K.; Yuan, X.; Cincio, L.; et al. Variational quantum algorithms. *Nat. Rev. Phys.* **2021**, *3*, 625−644.
(52) Tilly, J.; Chen, H.; Cao, S.; Picozzi, D.; Setia, K.; Li, Y.; Grant, E.; Wossnig, L.; Rungger, I.; Booth, G. H.; et al. The variational quantum eigensolver: a review of methods and best practices. *Phys. Rep.* **2022**, *986*, 1−128.
(53) Peruzzo, A.; McClean, J.; Shadbolt, P.; Yung, M.-H.; Zhou, X.-Q.; Love, P. J.; Aspuru-Guzik, A.; O'brien, J. L. A variational eigenvalue solver on a photonic quantum processor. *Nat. Commun.* **2014**, *5*, 4213.
(54) Wecker, D.; Hastings, M. B.; Troyer, M. Progress towards practical quantum variational algorithms. *Phys. Rev. A* **2015**, *92*, 042303.
(55) Kandala, A.; Mezzacapo, A.; Temme, K.; Takita, M.; Brink, M.; Chow, J. M.; Gambetta, J. M. Hardware-efficient variational quantum eigensolver for small molecules and quantum magnets. *Nature* **2017**, *549*, 242−246.
(56) Lee, J.; Huggins, W. J.; Head-Gordon, M.; Whaley, K. B. Generalized unitary coupled cluster wave functions for quantum computation. *J. Chem. Theory Comput.* **2019**, *15*, 311−324.
(57) Grimsley, H. R.; Economou, S. E.; Barnes, E.; Mayhall, N. J. An adaptive variational algorithm for exact molecular simulations on a quantum computer. *Nat. Commun.* **2019**, *10*, 3007.
(58) Sim, S.; Johnson, P. D.; Aspuru-Guzik, A. Expressibility and entangling capability of parameterized quantum circuits for hybrid quantum-classical algorithms. *Adv. Quantum Technol.* **2019**, *2*, 1900070.
(59) Zhang, S.-X.; Wan, Z.-Q.; Lee, C.-K.; Hsieh, C.-Y.; Zhang, S.; Yao, H. Variational quantum-neural hybrid eigensolver. *Phys. Rev. Lett.* **2022**, *128*, 120502.
(60) Fan, Y.; Liu, J.; Li, Z.; Yang, J. Quantum circuit matrix product state ansatz for large-scale simulations of molecules. *J. Chem. Theory Comput.* **2023**, *19*, 5407−5417.
(61) Zeng, X.; Fan, Y.; Liu, J.; Li, Z.; Yang, J. Quantum neural network inspired hardware adaptable ansatz for efficient quantum simulation of chemical systems. *J. Chem. Theory Comput.* **2023**, *19*, 8587−8597.
(62) Xiao, X.; Zhao, H.; Ren, J.; Fang, W.-H.; Li, Z. Physics-constrained hardware-efficient ansatz on quantum computers that is universal, systematically improvable, and size-consistent. *J. Chem. Theory Comput.* **2024**, *20*, 1912−1922.
(63) Li, W.; Zhang, S.-X.; Sheng, Z.; Gong, C.; Chen, J.; Shuai, Z. Quantum Machine Learning of Molecular Energies with Hybrid Quantum-Neural Wavefunction. *arXiv* **2025**, DOI: 10.48550/arXiv.2501.04264.
(64) Fang, J.-Y.; Guo, H. Multiconfiguration time-dependent Hartree studies of the CH3I/MgO photodissociation dynamics. *J. Chem. Phys.* **1994**, *101*, 5831−5840.
(65) McLachlan, A. D. A variational solution of the time-dependent Schrodinger equation. *Mol. Phys.* **1964**, *8*, 39−44.
(66) Sawaya, N. P.; Menke, T.; Kyaw, T. H.; Johri, S.; Aspuru-Guzik, A.; Guerreschi, G. G. Resource-efficient digital quantum simulation of d-level systems for photonic, vibrational, and spin-s Hamiltonians. *npj Quantum Information* **2020**, *6*, 49.
(67) Li, W.; Ren, J.; Huai, S.; Cai, T.; Shuai, Z.; Zhang, S. Efficient quantum simulation of electron-phonon systems by variational basis state encoder. *Phys. Rev. Res.* **2023**, *5*, 023046.
(68) Zhang, S.-X.; Allcock, J.; Wan, Z.-Q.; Liu, S.; Sun, J.; Yu, H.; Yang, X.-H.; Qiu, J.; Ye, Z.; Chen, Y.-Q.; et al. Tensorcircuit: a quantum software framework for the nisq era. *Quantum* **2023**, *7*, 912.

(69) Li, W.; Allcock, J.; Cheng, L.; Zhang, S.-X.; Chen, Y.-Q.; Mailoa, J. P.; Shuai, Z.; Zhang, S. TenCirChem: An efficient quantum computational chemistry package for the NISQ era. *J. Chem. Theory Comput.* **2023**, *19*, 3966−3981.
(70) McArdle, S.; Jones, T.; Endo, S.; Li, Y.; Benjamin, S. C.; Yuan, X. Variational ansatz-based quantum simulation of imaginary time evolution. *npj Quantum Information* **2019**, *5*, 75.
(71) Ollitrault, P. J.; Jandura, S.; Miessen, A.; Burghardt, I.; Martinazzo, R.; Tacchino, F.; Tavernelli, I. Quantum algorithms for grid-based variational time evolution. *Quantum* **2023**, *7*, 1139.
(72) Yao, Y.-X.; Gomes, N.; Zhang, F.; Wang, C.-Z.; Ho, K.-M.; Iadecola, T.; Orth, P. P. Adaptive variational quantum dynamics simulations. *PRX Quantum* **2021**, *2*, 030307.
(73) Zhang, Z.-J.; Sun, J.; Yuan, X.; Yung, M.-H. Low-depth Hamiltonian simulation by an adaptive product formula. *Phys. Rev. Lett.* **2023**, *130*, 040601.

https://doi.org/10.1021/acs.jpclett.5c00739
J. Phys. Chem. Lett. 2025, 16, 3911−3919